Solvent Dependence of the *N*-Methylacetamide Structure and Force Field

Valery Andrushchenko,[†] Pavel Matějka,[‡] David T. Anderson,[§] Jakub Kaminský,[†] Jan Horníček,[†,‡] Leif O. Paulson,[§] and Petr Bouř*[,†]

Institute of Organic Chemistry and Biochemistry, Academy of Sciences, Flemingovo nám. 2, 16610, Praha 6, Czech Republic, Department of Analytical Chemistry, Institute of Chemical Technology, Technická 5, 166 28, Prague 6, Czech Republic, and Department of Chemistry, University of Wyoming, 1000 East University Avenue, Laramie, Wyoming 82071

Received: May 15, 2009; Revised Manuscript Received: July 16, 2009

The *N*-methylacetamide molecule (NMA) is an important model for peptide and protein vibrational spectroscopy as it contains the main amide chromophore. In the past, some observed NMA geometry and spectral features could not be entirely explained at the harmonic level or by a single-conformer model. In particular, the spectra were found to be very dependent on molecular environment. In this work NMA Raman and infrared (IR) spectra in a variety of conditions were remeasured and simulated theoretically to separate the fundamental, dimer, and anharmonic bands. Under vacuum the MP2, MP4, and CCSD(T) wave function methods predicted a broad anharmonic potential energy well or even a double-well for the amide nitrogen out of plane motion, which density functional methods failed to reproduce. However, eventual nonplanar minima cannot support an asymmetric quantum state or explain band splittings observed in some experiments. In polar solvents the potential becomes more harmonic and the amide plane more rigid. On the other hand, solvent polarity enhances other anharmonic phenomena, such as the coupling between the carbonyl stretching (amide I) and lower frequency amide bending modes. The amide I band splitting is commonly observed experimentally. The influence of the CH_3 group rotations modeled by a rigid rotor model was found to be important for explaining some features of the spectra in a solid parahydrogen matrix. At room temperature the methyl rotation contributes to a nonspecific inhomogeneous band broadening. The dependence of the amide group flexibility on the environment polarity may have interesting consequences for peptide and protein folding studies.

Introduction

Vibrational spectroscopy of proteins and peptides is to a large extent based on the signal originating from the amide linkages. For example, different secondary structures of the same molecule provide differently shaped infrared absorption (IR) bands of the carbonyl stretching vibration ("amide I").[1] The difference is even more apparent in vibrational circular dichroism, where conformations provide characteristic sign patterns.[2] For the Raman scattering, the lower frequency modes, such as C−N stretching and N−H bending ("amide III"), are also used as structural marker bands.[3] The α-carbon of NMA is not substituted, unlike in most peptides, nevertheless the principal amide vibrations (amide A, I, II, and III) are localized and reasonably represented by this simplified system. Therefore, the *N*-methylacetamide (NMA) molecule attracted attention as a minimalistic model containing the amide −NHCO− residue embedded between two aliphatic carbon atoms (e.g., refs 4 and 5 and works cited therein).

However, the molecular structure, dynamics, and origin of all observable NMA bands are far from being completely understood. The molecule behaves differently in different environments and temperatures. For example, many Raman bands of pure NMA split at −120 °C, seven instead of the two expected fundamental bands appear within 1500−1700 cm^{-1}, some bands even change position by up to 20 cm^{-1} upon cooling, etc.[4] Possible nonplanarity of the amide bond in the ground state and its spectroscopic consequences have been discussed for a long time, but never proven.[6−11] Significant influence of hydration on electronic and vibrational NMA properties was predicted.[12] Lastly, methyl group rotation barriers were determined from a gas phase experiment[13] and rationalized by quantum computations.[14] The experimental 3-fold rotation barriers were determined as 73 and 79 cm^{-1} for the methyls attached to the carbon and nitrogen atoms, respectively. The rotations were never documented in a condensed state.

Alternative information about NMA vibrations could be obtained by the inelastic neutron scattering (INS), although this technique is oriented predominantly toward the solid state.[15] At the temperature of 4.5 K, an anomalous proton mode frequency was observed by INS if compared to IR and Raman spectroscopy data.[16] Further details were revealed about the lowest energy motions (e.g., methyl rotation), not accessible by optical spectroscopies.[17] Also the strong intermolecular NMA interaction mediated by the hydrogen bonds significantly influences the hydrogen vibration INS patterns,[18] similarly as for simpler amides.[19,20]

Strong anharmonic interactions are indicated by band splitting frequently observed in experimental Raman and IR spectra,[4,8,21,22] as well as by computational models.[23] A full-dimensional anharmonic computation significantly improved harmonic frequencies and provided estimates of the combination bands.[24] The anharmonicities are paramount for interpretation of 2D IR experiments.[25,26] The anharmonic splitting, however, is difficult to distinguish from the spectral changes caused by NMA aggregation in the condensed phase. The propensity of the

* To whom correspondence should be addressed. E-mail: bour@uochb.cas.cz.
† Academy of Sciences.
‡ Institute of Chemical Technology.
§ University of Wyoming.

10.1021/jp9045512 CCC: $40.75
Published on Web 08/07/2009

molecule to form dimers and longer chains complicates both liquid and solid pure NMA spectra,[4] and can also be observed in concentrated solutions.[27−31] In the pure liquid NMA, the population of the monomers is negligible and the structure is dominated by the linear associates.[30,31] Molecular dynamics and ab initio simulations, however, also attribute some band splitting to various types of solvent−solute hydrogen bonds.[22,32−34]

On the other hand, the cis−trans isomerization is well understood and the cis-isomer can be identified in IR spectra at elevated temperatures.[13,21] It is generally accepted, that under room temperatures and in solutions the trans form is energetically more convenient and dominant.[11,35−37]

In this study, we calculated equilibrium NMA geometry in various environments simulated by a polarizable continuum dielectric model[38] at different approximation levels. In line with previous works,[7] we conclude that the equilibrium Bohr−Oppenheimer geometry is probably planar in vacuum. However, the potential is strongly anharmonic, indicating an x^4 rather than an x^2 dependence. Eventual nonplanar minima suggested by some MP2, MP4, and CCSD(T) calculations do not support quantum states, and a planar structure quickly stabilizes in polar solvents. Similarly, we show that the potential energy landscape formed by methyl rotations also depends on the polarity of the environment, so that lowest energy conformers in vacuum and a condensed phase are different. As a next step we model the solvent dependence of the vibrational spectra at the harmonic approximation and beyond, and relate the predictions to experiments. It appears that the lower frequency motions are not so much coupled with the higher frequency normal modes, where the theoretical predictions are in good agreement with the experiment. We hope that the results shed some light on the complexity of the amide group vibrations and confirm the potential of the vibrational spectroscopy to study fine structure and dynamics of molecules.

Methods

Solution Spectra. *N*-Methylacetamide (NMA) (99+% purity) and all solvents (99% purity, ACS grade) were purchased from Sigma-Aldrich. The NMA solutions in various concentrations (% v/v) were prepared immediately before the measurements. To avoid formation of dimers and higher oligomers, a low NMA concentration was used for IR. Typically it was between 0.1% v/v and 1% v/v depending on the NMA propensity for dimerization in a particular solvent. A higher concentration (1−10% v/v) was used for the Raman scattering due to lower sensitivity of this technique; in this case the spectra might be slightly influenced by the dimerization.

The IR absorption spectra were acquired with an Equinox 55 FTIR spectrophotometer (Bruker Optics, Inc.) equipped with a DTGS detector, using a BaF_2 cell with a path length 35 μm, at room temperature (~22 °C). The path length was determined by counting the number of interference fringes measured with an empty cell. A total of 256 scans were accumulated for each spectrum at 4 cm^{-1} resolution. All spectral accumulations were repeated several times at identical conditions to ensure the reliability of the data and stability of the sample. All spectral manipulations were done with Opus software (Bruker Optics, Inc.). Water vapor traces were removed by the Atmospheric Water Compensation subroutine in Opus. Solvent spectra obtained under the same conditions were subtracted.

The FT Raman spectra were recorded with an Equinox 55/S FTIR/FTNIR spectrometer (Bruker Optics, Inc.) equipped with FT Raman module FRA 106/S (Bruker Optics, Inc.). The samples in glass vials were irradiated by a focused laser beam from a Nd:YAG laser (350 mW, 1064 nm, Coherent). Scattered light was collected in backscattering geometry. A quartz beamsplitter and liquid N_2 cooled Ge detector were used to obtain interferograms. A total of 1024 scans were accumulated and transformed by using Fourier transformation with a Blackmann−Harris cosine apodization function to obtain an individual spectrum at 2 cm^{-1} resolution. Twenty to fifty spectra per sample were collected repeatedly under identical experimental conditions. Subsequently, the spectral averages and standard deviation records were calculated and evaluated. The spectra were accumulated and processed with use of Opus. Solvent spectra obtained under the same conditions were subtracted.

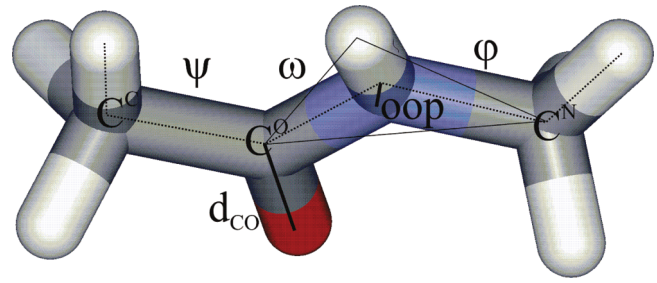

Figure 1. The *N*-methylacetamide molecule and selected geometry parameters: CO bond length (d_{CO}), the ψ ($\angle HC^CC^ON$), ω ($\angle C^CC^ONC^N$), and φ ($\angle C^ONC^NH$) dihedral angles, and the out-of-plane deviation (oop) of the nitrogen atom.

Parahydrogen Matrix Spectra. A low-temperature cryostat and high-resolution FTIR spectrometer were used to record spectra of NMA solvated in solid parahydrogen. Parahydrogen crystals doped with low concentrations of NMA are grown by using the "rapid vapor deposition" method developed by Fajardo and co-workers[39,40] that has been described elsewhere.[41,42] Independent gas flows of NMA and parahydrogen are co-deposited onto a BaF_2 optical substrate under cryogenic conditions. The hydrogen solid is enriched to 99.9% parahydrogen by using an ortho/para converter prior to deposition.[41,42] Further details of the amide I mode of NMA isolated in solid parahydrogen will be provided in a separate publication.[43] In the IR spectra reported here all non-NMA absorptions (impurities and solid parahydrogen absorptions) were removed to permit comparison with calculated spectra.

Harmonic Approximation. Equilibrium NMA (Figure 1) molecular geometry was obtained by energy minimization with the GAUSSIAN,[44] TURBOMOLE[45] (MP2 and DFT calculations), and ACESII[46] (CCSD(T) method) program packages. The approximation levels and basis sets are indicated below. The COSMO polarizable continuum solvent correction[47] was applied in some cases to model the environment as implemented in GAUSSIAN (where it is referred to as CPCM) and TURBOMOLE. To identify dimer bands in the experimental spectra, IR and Raman intensities of *trans*-NMA dimer were calculated at the MP2/6-311++G** level.

Anharmonic Vibrational Energies. The S4 program[48] interfaced to GAUSSIAN was used for a variational calculations of the vibrational frequencies and Raman and ROA intensities, based on a fourth-order Taylor expansion of the potential. The cubic and semidiagonal "*iijk*" quartic potential terms[49,50] were determined from the harmonic force fields by a numerical differentiation in normal mode coordinates, using a step approximately corresponding to a maximum Cartesian displacement of 0.05 Å. Previous works indicate that displacement magnitudes within ~0.001−0.1 Å provide relatively stable results for most systems.[51−53] Harmonic oscillator vibrational

TABLE 1: Equilibrium NMA Geometry Parameters Obtained with Various Computational Models

level	PCM solvent (ε_r)	oop (Å)	ψ (deg)	ω (deg)	φ (deg)	d_{CO} (Å)
HF/6-311++G**	vacuum (1)	0.000	0	180	180	1.1982
LSDA/6-311++G**	vacuum (1)	0.000	0	180	0	1.2218
BPW91/6-311++G**	vacuum (1)	0.000	0	180	0	1.2310
B3LYP/6-311++G**	vacuum (1)	0.000	0	180	0	1.2211
MP2/6-311++G**	vacuum (1)	0.118	2	174	173	1.2256
MP2/aug-cc-pVTZ	vacuum (1)	0.000	0	180	180	1.2268
MP4/6-311++G**	vacuum (1)	0.147	0	173	172	1.2307
CCSD(T) /6-311G**	vacuum (1)	0.125	16	172	156	1.2209
MP2/6-311++G**	H (1.294)	0.094	10	174	176	1.2281
MP2/6-311++G**	Ar (1.43)	0.091	0	176	176	1.2289
MP2/6-311++G**	heptane (1.92)	0.064	0	177	177	1.2312
MP2/6-311++G**	cycloxehane (2.02)	0.063	0	177	177	1.2316
MP2/6-311++G**	$CHCl_3$ (4.9)	0.000	0	180	180	1.2363
MP2/6-311++G**	H_2O (78)	0.000	0	180	180	1.2403

functions φ were used in a vibrational configuration interaction (VCI)[54] selected so that (1) the maximum excitation number was smaller or equal to five and (2) the perturbational parameter $\eta = |\langle\varphi|V|f\rangle/(E_\varphi - E_f)|$ was smaller than 0.001 for ground and fundamental (monoexcited) states f (E_i are the unperturbed energies and V is the anharmonic potential). Additionally, six lowest frequency vibrations had to be blocked, i.e., their excitations were not considered in the harmonic oscillator basis, to avoid numerical instability of the VCI computations. The blocking can be partially justified by a restricted coupling of the high- and low-frequency molecular motions.[10,53,55]

Methyl Group Rotations. The aforementioned anharmonic treatment based on the Taylor expansion cannot be used for soft large-amplitude molecular motions. Instead, a free-rotator model was used to estimate the effect of the methyl rotations on the spectra. The angles ψ and φ (Figure 1) determining conformation of the methyl groups attached to the carbonyl carbon and nitrogen, respectively, were scanned with regular 10° increments within 0 to 120°, and all other coordinates relaxed at the levels specified below. For the resulting geometries harmonic force fields **F** ($3N \times 3N$ matrix, where N is the number of atoms), electric dipole derivatives[56] **P** ($3 \times 3N$), and polarizability derivatives[57] $\boldsymbol{\alpha}$ ($3 \times 3 \times 3N$) were calculated. Vibrational normal-mode frequencies $\boldsymbol{\omega}$ were obtained from **F** by the usual procedure.[58]

The dependencies on the torsional angles were fitted by Fourier expansions $X(\varphi,\psi) = \sum_{i=1\ldots3}\sum_{j=1\ldots3} x_{ij}g_j(\psi)g_j(\varphi)$, where X is an element of $\boldsymbol{\omega}$, **P**, or $\boldsymbol{\alpha}$, and the planar waves contained three orthonormal basis functions, $\{g_i(\varphi)\} = \{(2\pi)^{-1}, \pi^{-1}\cos(3\varphi), \pi^{-1}\sin(3\varphi)\}$. The expansion coefficients x_{ij} were obtained by a numerical integration, $x_{ij} = \int\int X g_i g_j \, d\varphi \, d\psi$.

Next, a vibrational−rotational Hamiltonian with dimensionless normal mode coordinates (p_i,q_i)[58] was adopted as

$$H_0 = \sum_{i=1}^{3N-6-2} \frac{\hbar\omega_i(\varphi,\psi)}{2}(p_i^2 + q_i^2) - \frac{\hbar^2}{2I}\sum_{i=1}^{2}\frac{\partial^2}{\partial\varphi_i^2} + \frac{V_{3,N}}{2}(1 - \cos(3\varphi)) + \frac{V_{3,C}}{2}(1 - \cos(3\psi))$$

where $N = 12$, $\hbar$ is the Planck constant, and the methyl rotational constant $(2I)^{-1} = 5.537$ cm^{-1}. Experimental values[14] were chosen for the rotation barriers of $V_{3,N} = 79$ cm^{-1} and $V_{3,C} = 73$ cm^{-1}. The eigenstates were expanded as sums of adiabatic (with separate vibrational and internal rotational parts) basis functions $|q_1\rangle\ldots|q_{3N-6-2}\rangle|\varphi\rangle_{m_1}|\psi\rangle_{m_2}$, where $|q_i\rangle$ are the harmonic oscillator functions (ground and first excited states were considered) and $|\varphi\rangle_{m_1}$ and $|\psi\rangle_{m_2}$ are the rotational functions with the quantum numbers m_1 and m_2. The rotational states were constructed from the basis functions $\{\cos(m\varphi), \sin(m\varphi)\}\otimes\{\cos(m\psi), \sin(m\psi)\}$, $m = 0\ldots m_{max}$, with $m_{max} = 5$. Note that in this basis the Hamiltonian matrix elements could be calculated analytically and the state energies could be obtained by a diagonalization. Similarly as for the one-dimensional case of toluene,[59] transition matrix elements needed for the spectral intensities were also calculated from the wave functions and the Fourier expansions of **P** and $\boldsymbol{\alpha}$.

Results and Discussion

Equilibrium Geometry. The NMA potential energy surface is very shallow in the first three normal modes: out-of-plane nitrogen deviation, and the two methyl rotations. As discussed previously[7,9] different approximate levels provide equilibria with differently oriented methyl groups. Indeed, the equilibrium geometry parameters (defined in Figure 1) listed in Table 1 vary according to the approximation used. The conformer obtained at the HF level (where $\varphi = 180°$) is more similar to that obtained with the correlated MP2, MP4, and CCSD(T) wave function methods than to the DFT structures. This indicated that the correlation energy as implemented in DFT may be missing some aspects needed to yield the correct NMA geometry. Additionally, the MP2, MP4, and CCSD(T) structures with the limited 6-311++G** basis set are lacking the planar symmetry of the others, exhibiting a considerable out-of-plane deviation (oop) of the nitrogen atom within 0.118−0.174 Å. The nonplanar conformers provide enantiomeric species, optical activity of which was thoroughly discussed in ref 9. With the MP2/6-311++G** method additional higher energy conformer (local minimum, separated by 0.4 kcal/mol, not shown) was obtained for $\psi = 9°$, $\omega = 178°$, and $\varphi = 13°$. In agreement with a previous study[24] the MP2/aug-cc-pVTZ level provides a planar equilibrium with a very flat potential. A higher correlated method with larger basis sets thus might provide slightly nonplanar equilibria; these, unfortunately, require computer means beyond our possibilities. However, when the molecule is submerged into a solvent environment simulated by the polarizable continuum, the propensity toward the nonplanar arrangement quickly diminishes. For example, for heptane oop = 0.064 Å and a planar structure is obtained for chloroform by MP2/6-311++G**.

The detailed dependence of the relative electronic energy on oop calculated with various models is plotted in Figure 2. We can see that the HF and B3LYP methods provide approximately

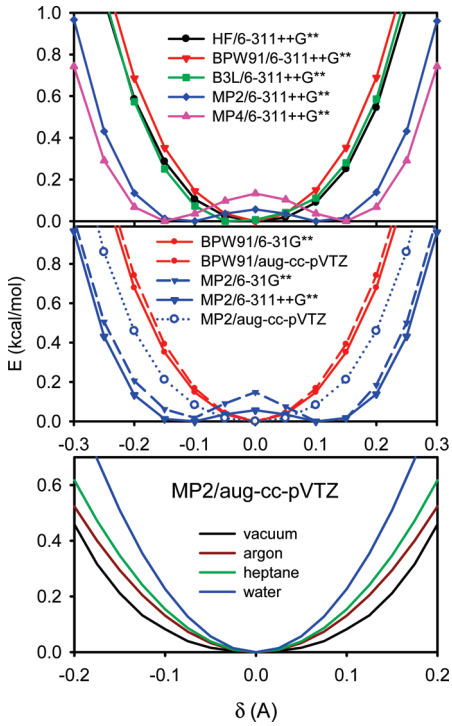

Figure 2. The dependence of the relative electronic energy on the NMA out-of-plane deviation (cf. Figure 1) as calculated at different levels and in various solvents (upper two panels are for vacuum, the MP4 single-point energies were obtained for the MP2/6-311++G** relaxed geometries).

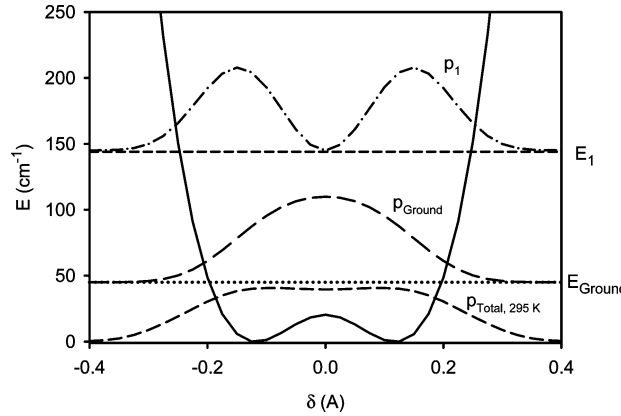

Figure 3. Energies of the ground and first vibrational state supported by the adiabatic out-of-plane MP2/6-311++G** potential, corresponding probabilities, and total probability at 295 K.

harmonic single-well potential, while the double-minima MP2 and MP4 curves are dramatically different. (For this scan MP2 relaxed geometries were used in the MP4 computations.) The MP4 method yields a more nonplanar structure than MP2, in agreement with the higher oop deviation obtained with this method (Table 1). This is somewhat surprising as normally effects of the MP2 perturbation are moderated by higher orders.[60]

In the past, the BPW91 GGA functional was used to simulate peptide vibrational spectra more efficiently than the hybrid (B3LYP) functionals.[61,62] The BPW91 method provides a potential only slightly affected by the basis set size (cf. middle panel of Figure 2), similar to B3LYP and HF (not shown). On the other hand, the MP2 level with the larger 6-311++G** basis yields a smaller oop barrier than with the 6-31G** basis set. The barrier further diminishes to zero for the aug-cc-pVTZ basis, but the flatness of the potential is conserved. Virtually the same energies were obtained in control single-point computations with the larger aug-cc-pVQZ basis; the MP2 method extrapolated to infinite basis set thus probably provides a one-minimum potential. In all cases the relaxation of the remaining degrees of freedom was found essential for the correct reproduction of the potential; the oop motion thus significantly couples with other molecular coordinates.

The oop amide potential is significantly dependent on molecular environment. The influence of the solvent is modeled by the polarizable continuum for argon, heptane, and water in the bottom panel of Figure 2 at the MP2/aug-cc-pVTZ level. As the polarity of the solvent grows the curve becomes sharper and more harmonic. The flexibility of the amide group is thus significantly decreased in polar environments.

None of the computations, however, suggests that an oop barrier between the two minima be high enough to support a localized quantum state with a longer lifetime, or even a split ground state level. Instead, the solution of the one-dimensional Schrödinger equation in the curvilinear oop coordinate[63−65] yields a broad probability distribution for the ground state reflecting the potential shape. An example is given in Figure 3 where the vibrational wave functions and probability are simulated for the extreme case of the MP2/6-311++G** double-well potential. Although the resulting probability at 295 K exhibits two maxima, the ground state energy is readily above the potential barrier.

Other motions are affected by the environment, too. The dependence of the energy on the methyl rotation described by angles ψ and φ is plotted in Figure 4. Under vacuum the B3LYP and BPW91 DFT methods provide symmetric minima, while the MP2 calculation leads to a two-minima pattern, asymmetric due to the oop flipping.[9] The methyl rotation barriers also vary, but all computations provide reasonable values (~80 cm^{-1} for both angles) with respect to the experimental numbers (73 and 79 cm^{-1}).[13] The DFT vacuum equilibrium ($\varphi = 0°$), however, shifts to 60° in the condensed phase (bottom of Figure 4). The potential energy surface obtained for H_2 is particularly interesting, being a nearly transitional state with almost free rotation of the φ angle. This can perhaps explain some low-temperature dynamical effects observed as fine features in the FTIR spectra.[43]

The geometry predictions obtained by various methods can partially be verified also by comparison to the experimental rotational constants (Table 2). The planar MP2/aug-cc-pVTZ geometry provides the best agreement with the experiment, although the precision is rather limited. It should also be noted that various semirigid rotor models give slightly different experimental values.[13] The largest A constant associated with the smallest moment of inertia perpendicular to the amide plane that is the most sensitive to the computational model and amide nonplanarity also indicates best agreement for the planar structures.

We can thus conclude that the effective NMA geometry under vacuum is planar in agreement with some earlier conclusions,[7] but the potential is flat and the more advanced correlated wave function method might provide a residual nonplanarity for the equilibrium. In solutions, where it could potentially be detected more easily, e.g., via optical activity,[9] the nonplanarity is even less probable. As discussed before, the amide group can easily be made nonplanar if placed in a chiral environment, e.g., in peptides and proteins.[11] For an ensemble of molecules, the flat character of the potential is reflected in the probability distribution (Figure 3). Both quantum and classical averaging provide planar geometry of NMA.

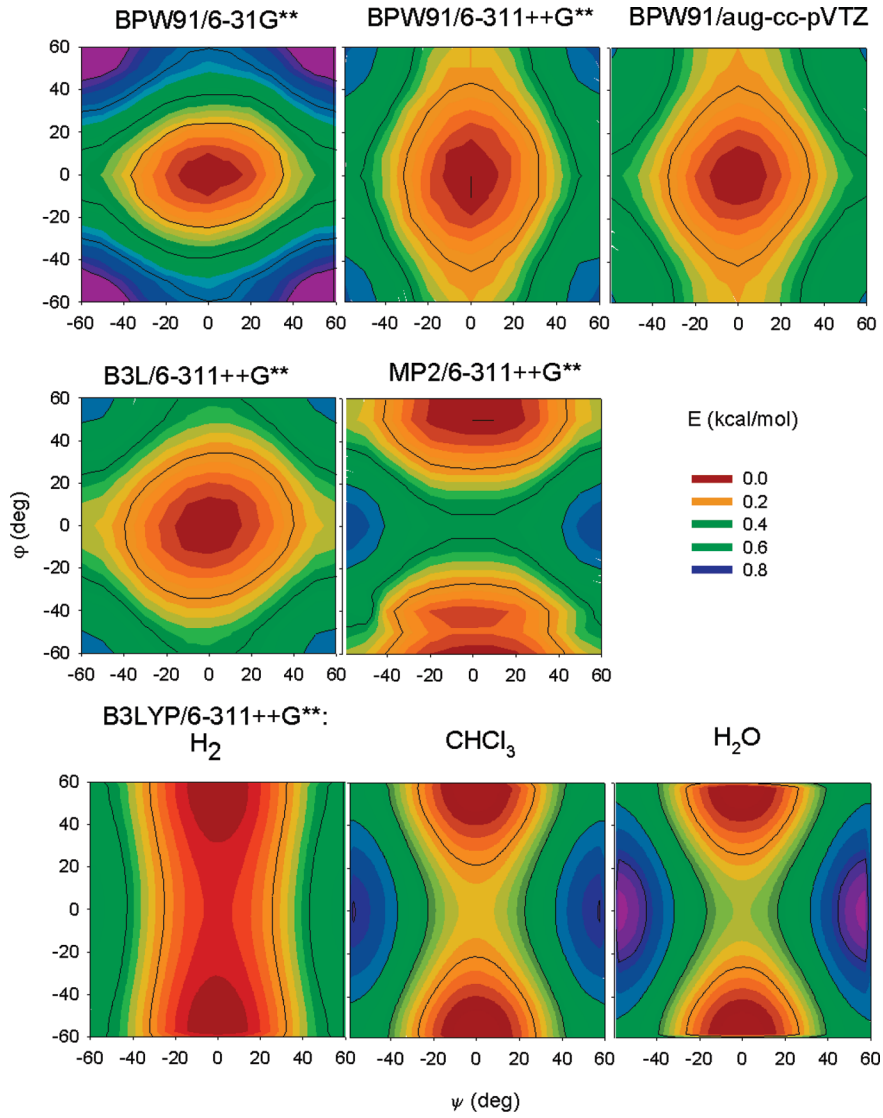

Figure 4. NMA potential energy as a function of the two methyl rotation angles (Figure 1) calculated at eight approximation levels, constructed from regular 13 × 13 grid points. Other coordinates were fully relaxed.

TABLE 2: Calculated and Experimental[a] NMA Rotational Constants (MHz)

level	*A*	*B*	*C*	δ
BPW91/6-31G**	9819	3808	2842	160
HF/6-311++G**	10402	3886	2930	89
LSDA/6-311++G**	10098	3946	2943	55
BPW/6-311++G**	9876	3800	2843	144
B3LYP/6-311++G**	10026	3820	2865	80
MP2/6-311++G**	10019	3882	2902	49
MP2/6-311++G**[b]	10022	3887	2907	49
MP2/aug-cc-pVTZ	10106	3908	2920	32
MP4/6-311++G**	9919	3851	2879	99
CCSD(T)/6-311G**	9934	3865	2888	88
exptl	10162(2)	3885(4)	2903(5)	0

[a] From jet-cooled FT microwave spectra.[13] [b] Averaged over the oop coordinate.

Solvent Dependence of Harmonic Frequencies. As discussed previously,[4,28,31,34,35,66−68] vibrational NMA spectra are very sensitive to the environment. The out-of-plane nitrogen motion and the hydrogen out-of-plane bending associated with the nonplanarity and nitrogen pyramidicity deserve special attention. Note that these two motions give rise to two distinct normal modes. They are also differently sensitive to the oop deviation. The H(N) bending calculated at the MP2/6-311++G** level for the equilibrium geometry at 381 cm^{-1} shifts to 260 cm^{-1} for a planar nonequilibrium ($\delta = 0$) structure. The frequency of the nitrogen oop motion (approximately the same as the oop coordinate in Figures 2 and 3) calculated at this level is positive (167 cm^{-1}) for the equilibrium and imaginary (i160 cm^{-1}) in the planar case. These vibrations are difficult to study experimentally as the low-frequency region is not easily accessible to measurement and might be obscured by a solvent signal; the hydrogen bending frequency is additionally extremely sensitive to hydrogen bonding.[20,49] More easily accessible higher frequency vibrations are less sensitive to the nonplanarity; the CO stretching, for example, changes by ∼3 cm^{-1} only.

The dependence of the vibrational transitions on the solvent obtained from the Raman and IR spectra is summarized in Table 3. It complements previous works, where especially the amide mode environmental dependence is discussed in detail.[4,6,21,28] The amide interacts strongly with the solvent via electrostatic interactions and hydrogen bonding. Nevertheless, we can see that frequencies for most modes are quite dependent on the solvent as well, including vibrations of the hydrophobic methyl groups traditionally considered as relatively indifferent to the

TABLE 3: Transition Frequencies of NMA Fundamental Vibrations in Various Environments

		exptl								
vibration	calcd vac[a]	vac[b]	H_2	N_2[c]	C_6H_{12}	CCl_4	$CHCl_3$	CH_3CN	NMA[d]	H_2O
amide A	3689	3545	3500	3498	3475	3474	3467	3380	3300	3229
amide I	1759	1725	1708	1707	1658	1651	1670	1673	1650	1639
amide II	1562	1501	1518	1511	1556	1535	1532	1566	1560	1582
δ(CH)	1528		1473	1472						
δ(CH)	1504		1449	1445						1454
δ(CH)	1498		1444	1432		1446	1446			1438
δ(CH)	1488		1442	1419						1420
N−CH_3 umbrela	1471		1419	1399		1414	1416		1412	1418
C−CH_3 umbrela	1411	1377	1368	1370	1363	1372	1370		1371	1379
amide III	1291	1255	1261	1266	1257	1303	1275	1290	1300	1317
N−CH_3 wag., ν(N$^{\alpha}$C)	1199	1185		1189	1160	1161	1165	1164	1160	1167
CH_3 wag.	1165			1169		1131		1096		
ν(N$^{\alpha}$C)	1121	1105	1089	1095		1098	1090			
C(O) oop, methyl wag	1057	1045	1040	1037	1039	1041	1039			
CH_3 wag	1006	970	983	980		971	980	985	989	999
δ(CNC), N−CH_3 wag	886	810	860	857	883	882	867	875	882	881
C(O) oop	639	625		619		637	670	626	628	
C(O) oop	616			439	627	628			599	633
C−C−N bend	427			429		447	366	436	438	
H(N) oop	381					437				
bend	264			279		299	261	284	293	
N oop	167					186		188	196	
combination band	3435[e]						3666			
dimer bands	3538					3300	3320			
						3102	3107			
	1730					1652	1655			
	1599					1565	1561			
	1323					1300	1299			
						989	985			

[a] MP2/6-311++G**, harmonic. [b] Reference 28. [c] Reference 21. [d] Reference 69. [e] PCM($CHCl_3$) solvent model.

TABLE 4: Average RMS Errors of Calculated Frequencies (Based on the Experimental Values in Table *3* over the Entire Range of Solvents)

method		δ (cm^{-1})
B3LYP/6-311++G**	harmonic	49
B3LYP/6-311++G**	anharmonic	40
MP2/6-311++G**	harmonic	65
MP2/6-311++G**	anharmonic	37

environment. The methyls are perhaps partially influenced by the solvent via its interaction with the amide moiety. From the concentration dependence of the spectra in the CCl_4 and $CHCl_3$ solvents bands corresponding to the dimer could be clearly separated. Their relative frequencies correspond well to the theoretical (MP2/6-311++G**) predictions; however, detailed analysis of the dimer vibrations goes beyond the scope of the present study. Likewise, it is currently difficult to assign the combination bands that are most frequently occurring at the high-wavenumber region (>2900 cm^{-1}).

For brevity, we skip a detailed list of the harmonic and anharmonic frequencies calculated for different solvents. The trends in calculated frequencies correspond very well to the experimental observations. The average root-mean-square (rms) errors are summarized in Table 4 for various approximation levels and the 6-311++G** basis set. Except for the lowest energy mode, this basis set provides frequencies very similar (within ~10 cm^{-1}) to those obtained with the larger aug-cc-pVTZ method, for example (cf. the vacuum frequencies in Table 3 and in ref 24). The B3LYP computation seems to provide better harmonic frequencies, but this advantage against MP2 is lost when the anharmonicity is included. Overall, both methods provide a reasonable agreement and also the dependence on

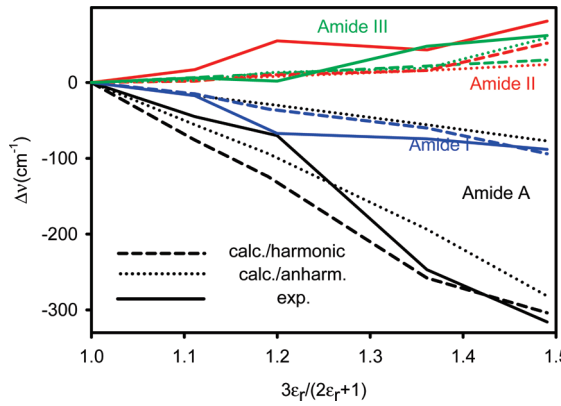

Figure 5. Calculated and experimental dependence of selected NMA vibrations on the relative permittivity of the environment.

the solvent. This is also documented in Figure 5 for the amide modes, where the experimental and MP2 wavenumber changes caused by the solvent as compared to the vacuum are plotted as a function of the Lorentz dielectric factor $3\varepsilon_r/(2\varepsilon_r + 1)$, where ε_r is the relative permittivity. The anharmonic correction does not significantly improve the dependence in this case. The nonlinear experimental dependencies may indicate a role of specific solvent−solute interactions, such as hydrogen bonding, not currently included in the PCM solvent model.

Somewhat surprising is the huge effect of the electron correlation on the amide harmonic frequencies summarized in Table 5 for the HF (= "MP0"), MP2, and MP4 methods and the 6-311++G** basis. Clearly, the MP2 level often taken as a standard provides results far from being converged; for example, the MP2 amide I frequency (1759 cm^{-1}) still changes

TABLE 5: The Influence of Electron Correlation on NMA Harmonic Frequencies (cm^{-1})

method	HF[a]	MP2[a]	MP4[a]	exptl[b]
amide A	3909	3689	3651	3545
$\nu(C-H)_{asym}$	3264	3166	3124	3000
$\nu(C-H)_{sym}$	3187	3081	3043	2917
amide I	1912	1759	1716	1725
amide II	1689	1562	1547	1501
amide III	1386	1291	1277	1255

[a] 6-311++G** basis set. [b] Experimental transition frequencies (ν(C−H) estimated for H_2 matrix, the rest for vacuum).

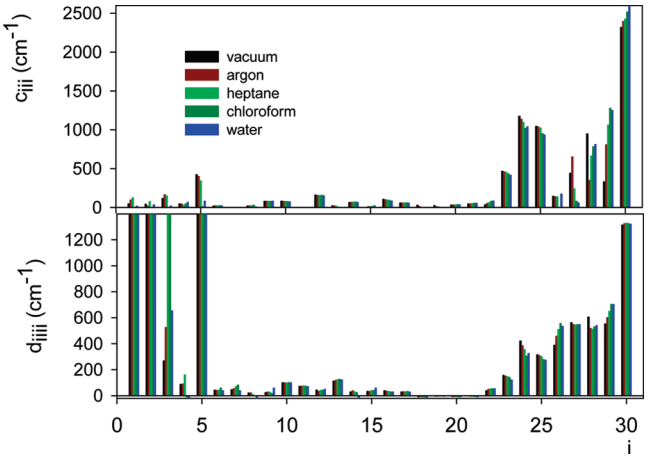

Figure 6. Diagonal cubic (c_{iii}) and quartic (d_{iiii}) normal mode constants for NMA calculated at the MP2/6-311++G**/CPCM level for different solvents.

to 1716 cm^{-1} for the higher order MP4 perturbation. The amide modes and the electronically simpler CH stretching behave similarly. Viewed from another perspective, the slow convergence of the computationally tedious wave function methods might have contributed to the success of the more empirical DFT modeling of peptide vibrations.

Anharmonic Interactions. Except for the lowest frequency modes, the anharmonic NMA constants exhibit a relatively modest dependence on the environment. This is documented in Figure 6 for the diagonal cubic c_{iii} and quartic d_{iiii} constants calculated (MP2/6-311++G**/CPCM) in five different solvents. The anharmonic constants are very large for the nitrogen and hydrogen out-of-plane bending modes (numbers 1 and 5), the methyl torsions (numbers 2 and 3), and all the hydrogen stretching modes (numbers 24−30). The CO stretching (number 23) in this respect behaves as an intermediate between the "harmonic" medium-frequency vibrations (∼400−1600 cm^{-1}) and the strongly anharmonic high-frequency hydrogen stretchings.

The anharmonic corrections cause a significant down-shift of most vibrations, regardless of the environment. This can be seen in Figure 7, where the simulated harmonic vacuum absorption NMA spectra are compared to the harmonic and anharmonic calculations for a hydrogen-like continuum and to the experiment recorded at the solid hydrogen matrix. In this case the anharmonic corrections are mostly larger than the solvent shifts; for some modes (amide III, ∼1260 cm^{-1}; amide II, ∼1520 cm^{-1}) they have even opposite sign. The amide A (NH stretching) is the most vulnerable as its calculated harmonic frequency (3689 cm^{-1}) changes to 3633 cm^{-1} in the H_2 dielectric, and further decreases to 3545 cm^{-1} with the anharmonic corrections, which reasonably well matches the experimental peak at 3500 cm^{-1}. Similarly, the C−H stretching frequencies within ∼2700−3100 cm^{-1} are best reproduced by the anharmonic calculation, although significant deviations still remain between the calculated and experimental intensity pattern. The higher frequency asymmetric stretches where one CH bond becomes longer and another one shorter seem to be "more harmonic", i.e., less shifted and split by the anharmonicities, than lower frequency nearly symmetric methyl CH stretches. Otherwise, in this region, the density of vibrational states is quite large and neither the used approximation, nor simple Taylor expansion of the nuclear potential, nor the anharmonic calculus oriented to the fundamental vibrations may be adequate to describe the fine spectral structure. The computed anharmonic shifts for the amide A, I, and III modes in H_2 (88, 11, and 31 cm^{-1}, respectively) are smaller than those obtained in this (118, 14, and 28 cm^{-1}) and previous[24] (160, 22, and 37 cm^{-1}) studies for vacuum.

Calculated anharmonic peaks of the amide A (∼3545 cm^{-1}) and I (1730 cm^{-1}) modes are accompanied by satellite bands from Fermi resonances. Although these cannot be unambiguously assigned to an experimental signal, the sensitivity of the amide I vibration to the resonances is in qualitative agreement with the H_2-matrix (Figure 7) and other[4,6,8,21,22] experiments, and seems to be a general property of the carbonyl group in amides.[6]

On the other hand, we presently cannot explain the amide II broadening observed in the experiment at ∼1520 cm^{-1}. In the gas[6,28] and nitrogen-matrix[21] NMA spectra the amide II center frequency is much more distinct. Therefore we suppose that the broadening is caused by a specific interaction with the hydrogen lattice not included in the model. It is also interesting that the amide III vibration, although it is primarily composed from the same N−C stretching and N−H bending coordinates as amide II, provides a very sharp peak at 1261 cm^{-1}. Also some other bands within 800−1200 cm^{-1} may be broadened in an analogous way, but their experimental detection is problematic because of the weak signal.

The relatively small differences in the anharmonic constants for different solvents result in notable changes in spectral intensities. Not only the fundamental frequencies shift as in the harmonic model, but the Fermi resonances and consequent peak splitting change with the solvent polarity. This is documented in Figure 8 for three solvents, where the Raman spectra calculated with the anharmonic model (at the MP2/6-311++G**/CPCM level) are compared to experiment. In cyclohexane, the amide III band (calculated at 1277 cm^{-1}/experimentally at 1267 cm^{-1}) is most probably accompanied by a resonance band at 1302/1303 cm^{-1}. The calculated intensity of the resonance band increases in chloroform and diminishes in water, in agreement with the experiment. In the C−H bending region (1400−1500 cm^{-1}) the calculated intensity is more spread in polar solvents; in water even a new distinct band at 1462 cm^{-1} appears. This trend is also apparent in the experimental spectra, although the water and chloroform signals are more similar than predicted.

The Raman amide II signal (∼1550−1570 cm^{-1}) is very weak and as expected for polar solvents[28] it shifts to higher frequencies. Finally, the calculated amide I band (∼1700 cm^{-1}) is accompanied by higher frequency satellite resonance bands, visible in both chloroform and cyclohexane experiments. In water, beside the higher frequency component, the central amide I band splits into three parts of comparable Raman intensities. They correspond to combination bands originating mostly in coupling of the CO stretching and NMA skeletal in-plane bending modes. They cannot be recognized in the experiment, but the overall broad character of the signal is in agreement with the simulation.

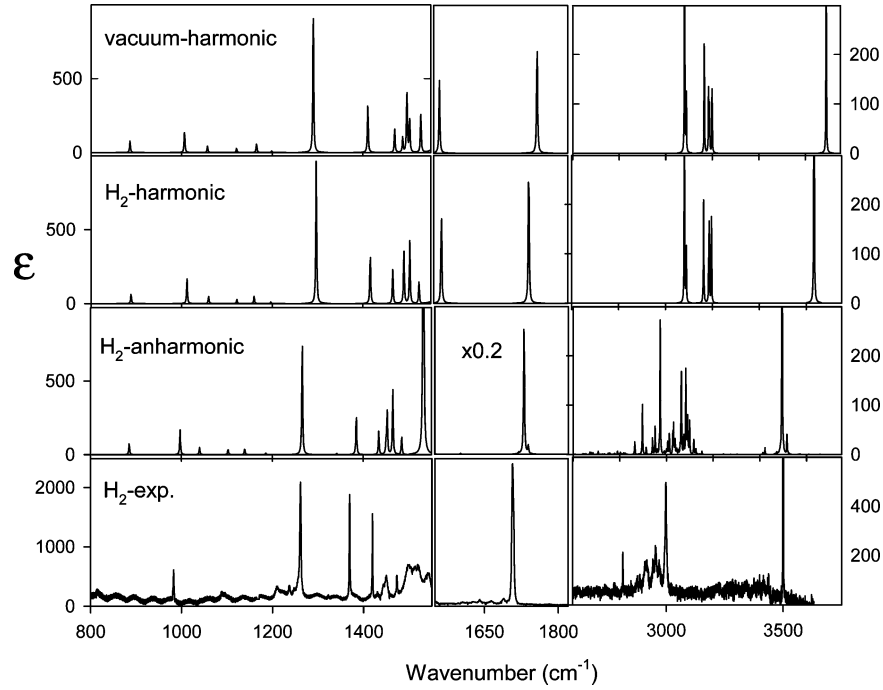

Figure 7. NMA absorption spectra calculated (MP2/6-311++G**/CPCM) in vacuum and in a hydrogen-like continuum at the harmonic and anharmonic level, as compared to the experimental spectrum recorded in solid-hydrogen matrix at 2 K. To facilitate the comparison, non-NMA signals were removed from the experiment.

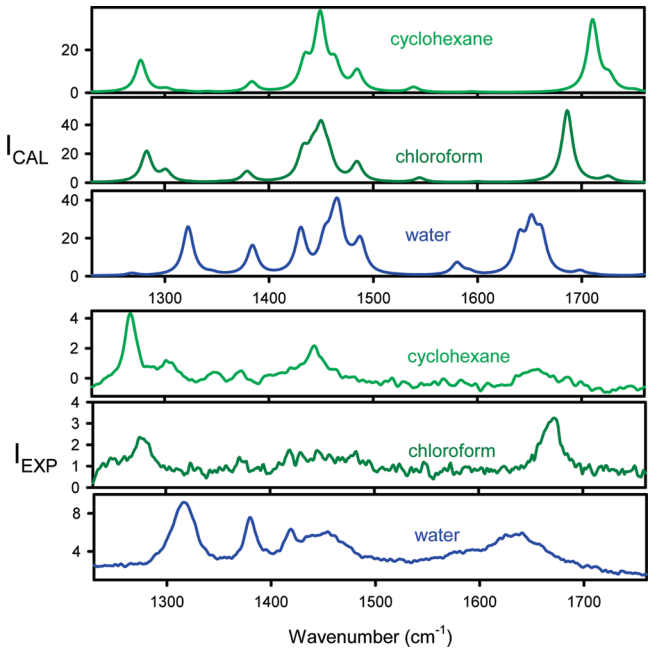

Figure 8. Calculated (top, MP2/6-311++G**/CPCM, anharmonic VCI calculation) and experimental (bottom) NMA Raman spectra.

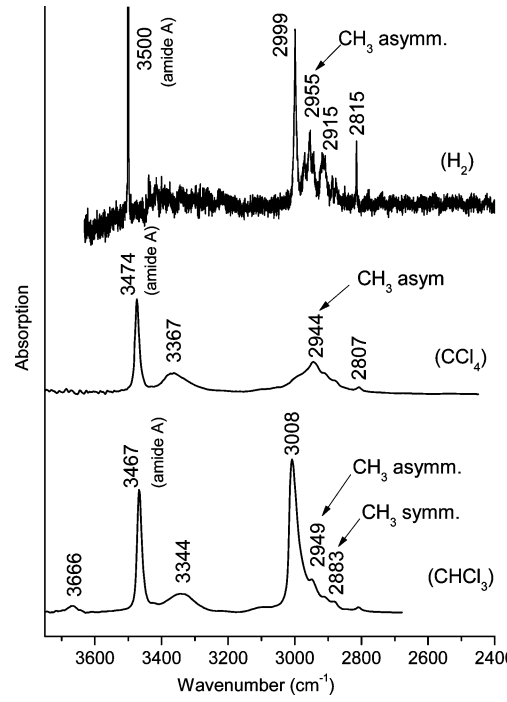

Figure 9. Experimental high-wavenumber IR spectra (in arbitrary intensity scale) of NMA in the hydrogen matrix, CCl_4, and $CHCl_3$ solvents.

The higher frequency region (>2400 cm^{-1}) is difficult to analyze as it is strongly anharmonic. In the three IR NMA spectra in the H_2 matrix, $CHCl_4$, and $CHCl_3$ solvents shown as an example in Figure 9, we can clearly identify the amide A band (2467−3500 cm^{-1}) and its wing (~3344−3367 cm^{-1}) corresponding to H-bound molecules. The C−H stretching bands around 3000 cm^{-1} have a relatively rich structure in the H_2 matrix. Similar splitting was observed in pure NMA at low temperatures.[4] At elevated temperatures (ref 4) and solutions (Figure 9) the bands are just broadened.

Methyl Group Rotation. Finally, we investigate the effects that the methyl rotation might have on the vibrational NMA spectra. Unlike for the toluene where the free rotation of methyl had clear consequences for the observable Raman signal,[59] we suppose that the quantum effects of the methyl NMA rotations at room temperature are covered by other effects stemming from stronger intermolecular interactions. However, an involvement of this motion beyond the harmonic approximation makes the spectral intensities somewhat more realistic for the low-temperature spectra in the hydrogen matrix.

The calculated (B3LYP/CPCM(H_2)/6-311++G**) absorption spectra in the harmonic approximation (Boltzmann average for

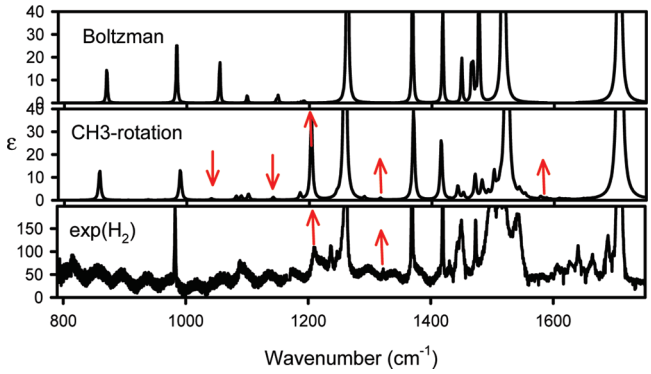

Figure 10. NMA Raman spectra calculated as Boltzmann harmonic average (top), with the CH_3 quantum free rotor model (middle), and the experimental spectrum in the H_2 matrix (bottom). The red arrows mark the most apparent changes caused by the rotation. The B3LYP/CPCM(H_2)/6-311++G** calculated fundamental frequencies were scaled (shifted) according to the experiment.

all CH_3 conformers) and with the rigid rotor model are compared to the experiment in Figure 10. The fundamental band frequencies in the theoretical spectra were scaled (shifted) according to the experimental ones. The anharmonic rigid rotor model causes many changes (some of them indicated by the red arrows in Figure 10) in the harmonic intensities in favor of the experiment: relative intensity of the 1040 and 1140 cm^{-1} band diminishes, while the intensity at 1183/1202 and 1308 cm^{-1} goes up. Also many new transitions appear, mostly around ~1310 and ~1610 cm^{-1}; although their band-to-band assignment is not possible, they qualitatively correspond to the rich experimental "background" signal. Thus we can conclude that the methyl rotation significantly contributes to the experimental signal and broadening of spectral lines, and its transitions are in principle detectable by the low-temperature matrix vibrational spectroscopy.

Conclusions

We have analyzed some aspects of the NMA dynamics and vibrational spectra to better understand the behavior of this molecule and the amide bond in various environments. The computations revealed a previously unreported deficiency of the density functional methods to reproduce the flatness of the out-of-plane nitrogen bending potential. Electron correlation effects included in the MP2, MP4, and CCSD(T) methods lend an extra flexibility to the amide bond, which, however, is significantly diminished in polar solvents. This motion, however, is coupled with other vibrations too weakly to produce visible spectral changes. On the other hand, medium frequency (~500−1000 cm^{-1}) skeletal modes strongly couple with the C−O stretching and depending on the environment they frequently produce combination bands. Both the harmonic and anharmonic model, and the experimental results document a strong environmental dependence of frequencies and intensities for all vibrations. The dependence is mostly caused by nonspecific electrostatic interactions, to some extent modulated by hydrogen bonding and other solvent-specific binding. The rigid rotor model enabled estimating the contribution of the methyl group motion to the broadening of experimental bands; for the case of the matrix H_2 spectra some weak transitions could be identified and modeled, otherwise not reproducible by conventional Boltzmann averaging. The combination of IR, Raman spectroscopy, and theoretical analyses thus provided a more complete picture of the mechanical properties of NMA and, in final effect, of the role of the amide moiety in peptides and proteins.

Acknowledgment. The Czech Science Foundation (grants nos. 203/06/0420, 202/07/0732) and the Grant Agency of the Academy of Sciences (A400550702, M200550902) supported this research. We thank Jan Kubelka for providing raw gas phase NMA data.

References and Notes

(1) Haris, P. I. Fourier Transform Infrared Spectroscopic Studies of Peptides: Potentials and Pitfalls. In *Infrared Analysis of Peptides and Proteins: Principles and Applications*; ACS Symposium Series; Ram Singh, B., Ed.; American Chemical Society: Washington, DC, 2000; p 54.
(2) Keiderling, T. A. Peptide and protein conformational studies with vibrational circular dichroism and related spectroscopies. In *Circular Dichroism: Principles and Applications*, 2nd ed.; Berova, N., Nakanishi, K., Woody, R. W., Eds.; Wiley-VCH: New York, 2000; p 621.
(3) Bussian, B. M.; Sander, C. *Biochemistry* **1989**, *28*, 4271.
(4) Herrebout, W. A.; Clou, K.; Desseyn, H. O. *J. Phys. Chem. A* **2001**, *105*, 4865.
(5) Torii, H.; Tatsumi, T.; Tasumi, M. *J. Raman Spectrosc.* **1998**, *29*, 537.
(6) Jones, R. L. *J. Mol. Spectrosc.* **1963**, *11*, 411.
(7) Mirkin, N. G.; Krimm, S. *J. Mol. Struct. (THEOCHEM)* **1995**, *334*, 1.
(8) Baron, M. H.; Fillaux, F. *Can. J. Chem.* **1985**, *63*, 1473.
(9) Polavarapu, P. L.; Deng, Z. Y.; Ewig, C. S. *J. Phys. Chem.* **1994**, *98*, 9919.
(10) Chalupský, J.; Vondrášek, J.; Špirko, V. *J. Phys. Chem. A* **2008**, *112*, 693.
(11) Bednárová, L.; Maloň, P.; Bouř, P. *Chirality* **2007**, *19*, 775.
(12) Ham, S.; Kim, J. H.; Kochan, L.; Cho, M. *J. Chem. Phys.* **2003**, *118*, 3491.
(13) Ohashi, N.; Hougen, J. T.; Suenram, R. D.; Lovas, F. J.; Kawashima, Y.; Fujitake, M.; Pyka, J. *J. Mol. Spectrosc.* **2004**, *227*, 28.
(14) Plusquellic, D. F.; Pratt, D. W. *J. Phys. Chem. A* **2007**, *111*, 7391.
(15) Fillaux, F. *Phys. B* **1995**, *213*, 619.
(16) Fillaux, F.; Baron, M. H.; Mayers, J.; Tomkinson, J. *Chem. Phys. Lett.* **1995**, *240*, 114.
(17) Barthes, M.; Bordallo, H. N.; Eckert, J.; Maurus, O.; de Nunzio, G.; Léon, J. *J. Phys. Chem. B* **1998**, *102*, 6177.
(18) Trabelsi, S.; Nasr, S.; Bahri, M.; Bellisent-Funnel, M. *J. Phys. Chem. B* **2006**, *110*, 25021.
(19) Bouř, P.; Tam, C. N.; Sopková, J.; Trouw, F. R. *J. Chem. Phys.* **1998**, *108*, 351.
(20) Tam, C. N.; Bouř, P.; Eckert, J.; Trouw, F. R. *J. Phys. Chem.* **1997**, *101*, 5877.
(21) Ataka, S.; Takeuchi, H.; Tasumi, M. *J. Mol. Struct.* **1984**, *113*, 147.
(22) DeCamp, M. F.; DeFlores, L.; McCracken, J. M.; Tokmakoff, A.; Kwac, K.; Cho, M. *J. Phys. Chem. B* **2005**, *2005*, 11016.
(23) Fujisaki, H.; Yagi, K.; Hirao, K.; Straub, J. E. *Chem. Phys. Lett.* **2007**, *443*, 6.
(24) Kaledin, A. L.; Bowman, J. M. *J. Phys. Chem. A* **2007**, *111*, 5593.
(25) Deflores, L. P.; Ganim, Z.; Ackley, S. F.; Chung, H. S.; Tokmakoff, A. *J. Phys. Chem. B* **2006**, *110*, 18973.
(26) Ganim, Z.; Chung, H. S.; Smith, A. W.; Deflores, L. P.; Jones, K. C.; Tokmakoff, A. *Acc. Chem. Res.* **2008**, *41*, 432.
(27) Takekiyo, T.; Yoshimura, Y.; Ikeji, Y.; Hatano, N.; Koizumi, T. *J. Phys. Chem. B* **2008**, *112*, 13355.
(28) Kubelka, J.; Keiderling, T. A. *J. Phys. Chem. A* **2001**, *105*, 10922.
(29) Noda, I.; Liu, Y.; Ozaki, Y. *J. Phys. Chem.* **1996**, *100*, 8674.
(30) Czarnecki, M. A.; Haufa, K. Z. *J. Phys. Chem. A* **2005**, *109*, 1015.
(31) Schweitzer-Stenner, R.; Sieler, G.; Mirkin, N. G.; Krimm, S. *J. Phys. Chem.* **1998**, *102*, 118.
(32) Mirkin, N. G.; Krimm, S. *J. Mol. Struct.* **1996**, *377*, 219.
(33) Chen, X. G.; Schweitzer-Stenner, R.; Krimm, S.; Mirkin, N. G.; Asher, S. A. *J. Am. Chem. Soc.* **1994**, *116*, 11141.
(34) Han, W.-G.; Suhai, S. *J. Phys. Chem.* **1996**, *100*, 3942.
(35) Chen, X. G.; Schweitzer-Stenner, R.; Asher, S. A.; Mirkin, N. G.; Krimm, S. *J. Phys. Chem.* **1995**, *99*, 3074.
(36) Mirkin, N. G.; Krimm, S. *J. Am. Chem. Soc.* **1991**, *113*, 9742.
(37) Deetz, M. J.; Fahey, J. E.; Smith, B. D. *J. Phys. Org. Chem.* **2001**, *14*, 463.
(38) Cossi, M.; Rega, N.; Scalmani, G.; Barone, V. *J. Comput. Chem.* **2002**, *24*, 669.
(39) Fajardo, M. E.; Tam, S. *J. Chem. Phys.* **1998**, *108*, 4237.
(40) Tam, S.; Fajardo, M. E. *Rev. Sci. Instrum.* **1999**, *70*, 1926.
(41) Yoshioka, K.; Anderson, D. T. *J. Chem. Phys.* **2003**, *119*, 4731.
(42) Paulson, L. O.; Anderson, D. T. *J. Phys. Chem. A* **2009**, *113*, 1770.
(43) Paulson, L. O.; Anderson, D. T. In preparation 2009.
(44) Frisch, M. J.; Trucks, G. W.; Schlegel, H. B.; Scuseria, G. E.; Robb, M. A.; Cheeseman, J. R.; Montgomery, J. A., Jr.; Vreven, T.; Kudin, K. N.; Burant, J. C.; Millam, J. M.; Iyengar, S. S.; Tomasi, J.; Barone, V.;

Mennucci, B.; Cossi, M.; Scalmani, G.; Rega, N.; Petersson, G. A.; Nakatsuji, H.; Hada, M.; Ehara, M.; Toyota, K.; Fukuda, R.; Hasegawa, J.; Ishida, M.; Nakajima, T.; Honda, Y.; Kitao, O.; Nakai, H.; Klene, M.; Li, X.; Knox, J. E.; Hratchian, H. P.; Cross, J. B.; Bakken, V.; Adamo, C.; Jaramillo, J.; Gomperts, R.; Stratmann, R. E.; Yazyev, O.; Austin, A. J.; Cammi, R.; Pomelli, C.; Ochterski, J. W.; Ayala, P. Y.; Morokuma, K.; Voth, G. A.; Salvador, P.; Dannenberg, J. J.; Zakrzewski, V. G.; Dapprich, S.; Daniels, A. D.; Strain, M. C.; Farkas, O.; Malick, D. K.; Rabuck, A. D.; Raghavachari, K.; Foresman, J. B.; Ortiz, J. V.; Cui, Q.; Baboul, A. G.; Clifford, S.; Cioslowski, J.; Stefanov, B. B.; Liu, G.; Liashenko, A.; Piskorz, P.; Komaromi, I.; Martin, R. L.; Fox, D. J.; Keith, T.; Al-Laham, M. A.; Peng, C. Y.; Nanayakkara, A.; Challacombe, M.; Gill, P. M. W.; Johnson, B.; Chen, W.; Wong, M. W.; Gonzalez, C.; Pople, J. A. *Gaussian 03*, Revision C.02; Gaussian, Inc.: Wallingford, CT, 2004.

(45) Ahlrichs, R.; Bar, M.; Baron, H.-P.; Bauernschmitt, R.; Bocker, S.; Ehrig, M.; Eichkorn, K.; Elliot, S.; Furche, F.; Haase, F.; Haser, M.; Horn, H.; Huber, C.; Huniar, U.; Kattannek, M.; Kolmel, C.; Koolwitz, M.; May, K.; Ochsenfeld, C.; Ohm, H.; Schafer, A.; Schneider, U.; Treutler, O.; von Arnim, M.; Weigend, F.; Weis, P.; Weiss, H. *Turbomole*, version 5; Quantum Chemistry Group, University of Karlsruhe: Karlsruhe, Germany, 1998.

(46) Stanton, J. F.; Gauss, J.; Watts, J. D.; Szalay, P. G.; Bartlett, R. J. *ACESII*; Mainz, Austin, Budapest, 2007.

(47) Klamt, A.; Schuurmann, G. *J. Chem. Soc., Perkin Trans.* **1993**, *2*, 799.

(48) Bouř, P. *S4*; Academy of Sciences: Prague, Czech Republic, 1994.

(49) Bouř, P.; Bednárová, L. *J. Phys. Chem.* **1995**, *99*, 5961.

(50) Bouř, P. *J. Phys. Chem.* **1994**, *98*, 8862.

(51) Carbonniere, P.; Lucca, T.; Pouchan, C.; Rega, N.; Barone, V. *J. Comput. Chem.* **2005**, *26*, 384.

(52) Barone, V. *J. Phys. Chem. A* **2004**, *108*, 4146.

(53) Daněček, P.; Bouř, P. *J. Comput. Chem.* **2007**, *28*, 1617.

(54) Carter, S.; Bowman, J. M.; Handy, N. C. *Theor. Chem. Acc.* **1998**, *100*, 191.

(55) Daněček, P.; Bouř, P. *J. Chem. Phys.* **2007**, *126*, 224513.

(56) Stephens, P. J.; Devlin, F. J.; Ashvar, C. S.; Chabalowski, C. F.; Frisch, M. J. *Faraday Discuss.* **1994**, *99*, 103.

(57) Barron, L. D. *Molecular Light Scattering and Optical Activity*; Cambridge University Press: Cambridge, UK, 2004.

(58) Papoušek, D.; Aliev, M. R. *Molecular Vibrational/Rotational Spectra*; Academia: Prague, Czech Republic, 1982.

(59) Kapitán, J.; Hecht, L.; Bouř, P. *Phys. Chem. Chem. Phys.* **2008**, *10*, 1003.

(60) *The Encyclopedia of Computational Chemistry*; Schleyer, P.v. R., Allinger, N. L., Clark, T., Gasteiger, J., Kollman, P. A.; Schaefer, H. F., III, Schreiner, P. R., Eds.; John Wiley & Sons: Chichester, UK, 1998.

(61) Bouř, P.; Kubelka, J.; Keiderling, T. A. *Biopolymers* **2002**, *65*, 45.

(62) Bouř, P.; Keiderling, T. A. *J. Mol. Struct. (THEOCHEM)* **2004**, *675*, 95.

(63) Podolsky, B. *Phys. Rev.* **1928**, *32*, 812.

(64) Čejchan, A.; Špirko, V. *J. Mol. Spectrosc.* **2003**, *217*, 142.

(65) Bouř, P.; Buděšínský, M.; Špirko, V.; Kapitán, J.; Šebestík, J.; Sychrovský, V. *J. Am. Chem. Soc.* **2005**, *127*, 17079.

(66) Asher, S. A.; Li, P.; Chi, Z. H.; Chen, X. G.; Schweitzer-Stenner, R.; Mirkin, N. G.; Krimm, S. *J. Phys. Chem.* **1997**, *101*, 3992.

(67) Mennucci, B.; Martínez, J. M. *J. Phys. Chem. B* **2005**, *109*, 9818.

(68) Yang, S.; Cho, M. *J. Chem. Phys.* **2005**, *123*, 134503.

(69) Schrader, B. *Raman/Infrared Atlas of Organic Compounds*, 2nd ed.; VCH: Weinheim, Germany, 1989.

JP9045512